

# Characterization of the electronic properties of $\text{YB}_4$ and $\text{YB}_6$ using $^{11}\text{B}$ NMR and first-principles calculations

B. Jäger<sup>a</sup>, S. Paluch<sup>b</sup>, W. Wolf<sup>c</sup>, P. Herzig<sup>a</sup>, O. J. Żogał<sup>b</sup>,  
N. Shitsevalova<sup>d</sup>, Y. Paderno<sup>d</sup>

<sup>a</sup>*Institut für Physikalische Chemie, Universität Wien, Währinger Straße 42,  
1090 Vienna, Austria*

<sup>b</sup>*Institute for Low Temperature and Structure Research, Polish Academy of  
Sciences, P. O. Box 1410, 50-950 Wrocław, Poland*

<sup>c</sup>*Materials Design s. a. r. l., 44, av. F.-A. Bartholdi, 72000 Le Mans, France*

<sup>d</sup>*Institute for Problems of Materials Science, Academy of Sciences of Ukraine,  
3 Krzhyzhanovsky str., 03680 Kiev, Ukraine*

---

**Abstract**

Two compounds, tetragonal YB<sub>4</sub> and cubic YB<sub>6</sub>, have been investigated by electric-field gradient (EFG) and Knight shift measurements at the boron sites using the <sup>11</sup>B nuclear magnetic resonance (NMR) technique and by performing first-principles calculations. In YB<sub>6</sub> <sup>11</sup>B ( $I = 3/2$ ) NMR spectra reveal patterns typical for an axially symmetric field gradient with a quadrupole coupling frequency of  $\nu_Q = 600 \pm 15$  kHz. In the second boride (YB<sub>4</sub>) three different EFGs were observed corresponding to the three inequivalent crystallographic sites for the boron atoms ( $4h$ ,  $4e$ , and  $8j$ ). They correspond to:  $\nu_Q(4h) = 700 \pm 30$  kHz with an asymmetry parameter  $\eta = 0.02 \pm 0.02$ ,  $\nu_Q(4e) = 515 \pm 30$  kHz,  $\eta = 0.00 + 0.02 / - 0.00$ , and  $\nu_Q(8j) = 515 \pm 40$  kHz,  $\eta = 0.46 \pm 0.08$ . The Knight shifts measured by Magic-Angle Spinning (MAS) NMR at room temperature are very small being  $0.6 \pm 8$  ppm and  $-1 \pm 8$  ppm for YB<sub>4</sub> and YB<sub>6</sub>, respectively. For the theoretical calculations structure optimizations were performed as a first step. For the obtained structural parameters the EFGs were computed within the local-density approximation. Very satisfactory agreement between experimental and theoretical results is obtained both for the structural parameters and the B EFGs thus confirming the underlying structural models. In addition to the EFGs, band structures, densities of states, and valence-electron densities are presented and the bonding situation in the two yttrium borides is discussed. The band-structure results are compatible with the very low values for the Knight shifts mentioned above.

*Key words:* Metal borides; Electronic band structure; Electric field gradient; Chemical bonding; NMR

---

\* Corresponding author. Fax: +43-1-4277-9524.

*Email address:* peter.herzig@univie.ac.at (P. Herzig).

## 1 Introduction

Through their specific properties, transition metal borides became attractive both from scientific and technical point of view. For instance,  $\text{YB}_6$ , like some other rare-earth and actinide hexaborides, shows superconductivity below 7.1 K [1] and has been considered as a possible candidate for high-temperature thermoelectric materials [2].

Detailed knowledge of the electronic structure of a material is a key ingredient for an in-depth understanding of many of its macroscopic features. A combination of experimental methods as well as computations on an *ab-initio* level has proved very efficient, in particular relating electronic structure calculations to results of nuclear magnetic resonance (NMR) technique. The value of the electric field gradient (EFG), measured by NMR quadrupole interaction, is directly determined by the charge distribution around the nucleus. Thus, theoretical EFG studies based on the electronic structure are important in order to give a reliable interpretation of the experimental data. One of the strengths of NMR measurements is that, being a microscopic tool, they are sensitive to the symmetry of the crystallographic sites and in particular to the electron density in the vicinity of the nucleus. In a recent study, this sensitivity was used to provide criteria for the determination of crystal structures that are still under debate [3,4,5].

In the present paper, we report the EFG values for  $\text{YB}_6$  and  $\text{YB}_4$  and the determination of the Knight shifts by using the Magic-Angle Spinning (MAS) technique. The experimental EFGs are compared and interpreted with the theoretical ones obtained from *ab-initio* calculations.

The structure of cubic  $\text{YB}_6$  (space group  $Pm\bar{3}m$ , no. 221) consists of a simple cubic lattice of corner-connected  $\text{B}_6$  octahedra with Y atoms filling the cubic holes. In this and other borides with the same structure the B–B distance be-

tween neighbouring octahedra is slightly shorter than within the octahedron (for  $\text{YB}_6$ : 1.64 Å compared to 1.75 Å). In agreement with this crystallographic structure there is only a single EFG value. A previous  $^{11}\text{B}$  NMR study for  $\text{YB}_6$  [6] reported the spin-lattice relaxation time and the spectrum. However, the authors were unable to determine the EFG because of the widely broadened satellite lines and the weak NMR signal used in their instrumentation.

On the other hand, tetragonal  $\text{YB}_4$  (space group  $P4/mbm$ , no. 127) has a quasilayer structure with alternating sheets of Y atoms and  $\text{B}_6$  octahedra linked together laterally by  $\text{B}_2$  units. In this structure five different nearest-neighbour B–B distances between 1.64 Å and 1.81 Å are observed. In  $\text{YB}_4$  the boron atoms are situated in three different crystallographic positions with different EFGs for each of them, as will be demonstrated in the present paper.

## 2 Structure optimization

For confirmation of the validity of the available experimental lattice parameters and the atomic positions, calculations have been performed using the Vienna *ab-initio* simulation package (VASP) [7,8,9]. By this method the Kohn–Sham equations of density-functional theory [10,11] with periodic boundary conditions are solved within a plane-wave basis set with electron–ion interactions described by the projector augmented wave (PAW) method [12,13]. For exchange and correlation the general gradient approximation (GGA) [14] was applied. The structural parameters were calculated by atomic forces and stress-tensor minimization. For each of the two borides two different energy cutoffs for the plane-wave basis were used (400 eV and a cutoff higher by at least a factor of 2), which lead to practically the same results, so that adequate convergence is ensured. The experimental and calculated structural parameters for  $\text{YB}_4$  and  $\text{YB}_6$  are given in Tables 1 and 2, respectively. For cubic  $\text{YB}_6$ , where the lattice parameter  $a$  and the positional parameter of the B atom are

Table 1

Experimental and calculated structural parameters for  $\text{YB}_4$  adopting the  $\text{ThB}_4$  structure ( $P4/mbm$ , no. 127). The lattice parameters are in  $\text{\AA}$ .

Lattice parameters	Positional parameters	Atom	Site	Remarks
$a = 7.111$	$x = 0.3179$	Y	$4g$	exp., Ref. [15]
$c = 4.017$	$z = 0.2027$	B(1)	$4e$	
	$x = 0.0871$	B(2)	$4h$	
	$x = 0.1757$	B(3)	$8j$	
	$y = 0.0389$			
$a = 7.1035$				exp., Ref. [16]
$c = 4.0206$				
$a = 7.1091$	$x = 0.3182$	Y	$4g$	calc., VASP (GGA)
$c = 4.0280$	$z = 0.2030$	B(1)	$4e$	
	$x = 0.0870$	B(2)	$4h$	
	$x = 0.1760$	B(3)	$8j$	
	$y = 0.0386$			

the only free parameters, the minimum-energy structure was also found by the full-potential linearized augmented plane-wave (FLAPW) method within the LDA approximation which is described in the next Section.

The structural parameters optimized by VASP have been used to calculate the EFGs for  $\text{YB}_6$  and  $\text{YB}_4$ .

Table 2

Experimental and calculated structural parameters for  $\text{YB}_6$  adopting the  $\text{CaB}_6$  structure ( $Pm\bar{3}m$ , no. 221). The lattice parameters are in  $\text{\AA}$ , the positional parameter refers to site  $6f$  of B.

Lattice parameter $a$	Positional parameter $x$	Remarks
4.102		exp., Ref. [17]
4.1025	0.202	exp., Ref. [18]
4.113		exp., Ref. [19]
	0.199	exp., Ref. [20]
4.0436	0.1989	calc., FLAPW (LDA)
4.1004	0.1988	calc., VASP (GGA)

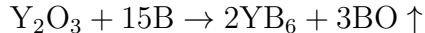
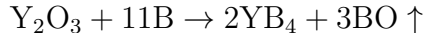
### 3 Electric-field gradients

#### 3.1 Experimental

To avoid skin-depth effects for better RF penetration, the samples were used in powder form and obtained by crushing the single crystals. The crystals were obtained by crucible free inductive zone melting of the  $\text{YB}_4$  and the  $\text{YB}_6$  source rods that provides a high purity and single-phase material. They, in turn, were prepared in the following steps:

- (1) Mixing of  $\text{Y}_2\text{O}_3$  (purity 99.999%) and boron components in proper ratios.
- (2) Synthesis of the  $\text{YB}_4$  and the  $\text{YB}_6$  powders by routine solid-state reaction

of borothermic reduction:



- (3) Slip casting of source rods, removal of the binder and sintering of the rods in the vacuum.

The  $^{11}\text{B}$  NMR experiments were carried out with a Bruker DSX Avance spectrometer at a frequency of 96.29 MHz. The static spectra were obtained by the Fourier transform of the free induction decay (FID) following a short single pulse (in the range of 0.9–2.5  $\mu\text{s}$ ). The spectra contain up to 256 accumulations with a repetition time of 20 s. A 4 mm MAS probe was used with rotation frequencies between 7 and 9 kHz. The chemical shifts are given with respect to external  $\text{BF}_3\text{Et}_2\text{O}$ . In Fig. 1 the  $^{11}\text{B}$  NMR spectra for  $\text{YB}_4$  and  $\text{YB}_6$  are given.

### 3.2 *First-principles calculations*

The all-electron band-structure calculations for the calculation of EFGs are based on the density-functional theory [10,11] (DFT) and the local-density approximation and have been performed by the linearized augmented plane-wave (LAPW) method [21] in its full-potential version [22,23,24,25] (FLAPW) using an exchange-correlation potential by Hedin and Lundqvist [26,27].

The EFGs have been calculated from the  $l = 2$  components of the Coulomb potential near the nuclei. The formalism by Herzig [28] and Blaha et al. [29] has also been employed to split the calculated EFG components into the contributions from the surrounding electrons within the respective muffin-tin sphere (“sphere contribution”) and the remainder that comes from outside this sphere (“lattice contribution”). This partitioning depends, to a small extent, on the

choice of the muffin-tin radii. The valence contribution can be split further into the allowed  $ll'$  contributions (only  $sd$ ,  $pp$ ,  $pf$  are important in the present context) which provide useful information about the influence of particular  $l$ -like wave functions on the EFGs [30]. As is common practice the EFG component with the largest absolute value is always designated as  $V_{zz}$ . For further algorithmic details on the EFG calculation see our recent paper [4].

### 3.3 EFGs: Results and discussion

Figure 1 shows the  $^{11}\text{B}$  spectra which are typical for a nuclear spin  $I = 3/2$  in the presence of first-order quadrupole effects. For  $\text{YB}_6$  (bottom of Fig. 1) the separation of the satellite lines is given by  $\delta\nu = \nu_Q (3 \cos^2 \Theta - 1)$ , where  $\Theta$  are the powder singularities.  $\Theta = 90^\circ$  thus yields  $\nu_Q = e^2qQ/2h$ . Here,  $eq = V_{zz}$  and  $Q$  is the largest component of the electric-field-gradient tensor and the nuclear quadrupole moment, respectively. The axially symmetric field gradient is consistent with the local symmetry at the boron site. The existence of three inequivalent boron sites in  $\text{YB}_4$  is the origin of the more complex satellite spectrum compared to  $\text{YB}_6$  (Fig. 1). The  $\nu_Q$  value and the asymmetry parameter  $\eta = (V_{xx} - V_{yy})/V_{zz}$  were obtained using the *dmfit* simulation program [31]. The  $\nu_Q$  value translates into  $C_q = 2\nu_Q$  and it follows for  $V_{zz} = 4.136 \times 10^{19} C_q/Q$  (in  $\text{V}/\text{m}^2$ ) when the appropriate  $Q$  value (in barns) for  $^{11}\text{B}$  is used and  $C_q$  is inserted in units of MHz. Since different nuclear quadrupole moments can be found in the literature, the experimental values for  $V_{zz}$  were determined for two different values, namely  $Q = 0.04$  b and  $Q = 0.0355$  b [32]. The former  $Q$  value has been taken from the almanac of the spectrometer manufacturer Bruker and is very close to  $Q = 0.04059$  [33] recommended by Pyykkö [34] in his compilation of nuclear quadrupole moments. The results are shown in Tables 3 and 4 for  $\text{YB}_6$  and  $\text{YB}_4$ , respectively. Experimentally only the absolute value of  $V_{zz}$  and  $\eta$  can be determined for the powder specimens.



Table 3

Calculated B EFGs (in  $10^{20}$  V/m<sup>2</sup>) for YB<sub>6</sub> for the optimized structure compared to the experimental results assuming an <sup>11</sup>B nuclear quadrupole moment of 0.04 and  $0.0355 |e| \times 10^{-28}$  m<sup>2</sup>, respectively.

Calc.	Exp.	Exp.
Opt. struct.	$Q = 0.04$	$Q = 0.0355$
$V_{zz}$	$ V_{zz} $	$ V_{zz} $
-13.5	$12.4 \pm 0.3$	$14.0 \pm 0.3$

Table 4

Calculated B EFGs (in  $10^{20}$  V/m<sup>2</sup>) for YB<sub>4</sub> for the experimental structure [15] and the optimized structure compared to the experimental results assuming an <sup>11</sup>B nuclear quadrupole moment of 0.04 and  $0.0355 |e| \times 10^{-28}$  m<sup>2</sup>, respectively.

		Calc.		Calc.		Exp.		Exp.	
		Exp. struct.		Opt. struct.		$Q = 0.04$		$Q = 0.0355$	
Site	$i$	$V_{ii}$	$\eta$	$V_{ii}$	$\eta$	$ V_{ii} $	$\eta$	$ V_{ii} $	$\eta$
B(1)	$z$	-11.0	0.0	-10.8	0.0	$10.6 \pm 0.6$	0.0	$12.0 \pm 0.6$	0.0
B(2)	$x$	-8.1		-8.2					
	$y$	-8.3		-8.4					
	$z$	16.4	0.02	16.6	0.01	$14.5 \pm 0.6$	0.02	$16.3 \pm 0.6$	0.02
B(3)	$x$	2.7		2.9					
	$y$	7.9		7.9					
	$z$	-10.6	0.48	-10.8	0.47	$10.6 \pm 0.9$	$0.46 \pm 0.09$	$12.0 \pm 0.9$	$0.46 \pm 0.08$

For YB<sub>6</sub> the B EFG corresponds to the axially symmetric case (site symmetry  $C_{4v}$ ) where there is only one independent EFG component. In YB<sub>4</sub> the situation is more complicated. The three crystallographically distinct B sites (site symmetries:  $C_4$  for B(1),  $C_{2v}$  for B(2), and  $C_s$  for B(3)) lead to one, two, and

Table 5

Split of the B EFG for YB<sub>6</sub> (optimized structure) into lattice and sphere components and the latter into its main contributions, i. e., *sd*, *pp*, and *pf*. All  $V_{zz}$  values are in units of  $10^{20}$  V/m<sup>2</sup>.

Site	$V_{zz}$	$V_{zz}^{lat}$	$V_{zz}^{sph}$	$V_{zz}^{sd}$	$V_{zz}^{pp}$	$V_{zz}^{pf}$
B	-13.5	9.0	-22.5	-1.9	-17.8	-2.3

three independent EFG components, respectively. This means that for B(2) and B(3) a non-zero asymmetry parameter  $\eta$  is observed.

The comparison between calculated and measured EFGs shows very good agreement, if the absolute values are considered. In general for the EFG tensor either one or two components are negative. The corresponding principal axes are determined by the strongest bonding interactions. In the case of YB<sub>4</sub> the negative EFG component for B(1) ( $V_{zz}$ ) is related to the axis of the inter-octahedral B–B bond along the *c* axis, for B(2) the two negative components ( $V_{xx}$  and  $V_{yy}$ ) refer to the (001) plane through B(2) and its three B neighbours, and finally for B(3) the negative EFG component ( $V_{zz}$ ) refers to the axis of the bond between the adjacent atoms of a B<sub>6</sub> octahedron and a B<sub>2</sub> unit.

Now the splits of the B EFGs into the lattice and sphere contributions and the latter into their main components (*sd*, *pp*, and *pf*) are considered (Tables 5 and 6). The sphere contribution is the one with the largest absolute value, but also the lattice contribution is relatively large. This behaviour has been observed previously for borides and other second-group elements by Schwarz et al. [35]. For the H atom in hydrides the lattice contribution is even larger than the sphere contribution, as has been found recently [4]. It is not surprising that the *pp* component dominates the sphere contribution with the *sd* and *pf* components being the largest other components.

Table 6

Split of the B EFGs for YB<sub>4</sub> (optimized structure) into lattice and sphere components and the latter into its main contributions, i. e., *sd*, *pp*, and *pf*. All  $V_{zz}$  values are in units of  $10^{20}$  V/m<sup>2</sup>.

Site	$V_{zz}$	$V_{zz}^{lat}$	$V_{zz}^{sph}$	$V_{zz}^{sd}$	$V_{zz}^{pp}$	$V_{zz}^{pf}$
B(1)	-10.8	7.2	-18.0	-1.4	-14.6	-1.7
B(2)	16.6	-4.0	20.6	1.3	17.8	1.3
B(3)	-10.8	5.0	-15.7	-1.3	-12.6	-1.6

### 3.4 Knight shifts

The Knight shifts,  $K$ , measured for both compounds, are found to be very small, i. e., 0.6 ppm and  $-1$  ppm for YB<sub>6</sub> and YB<sub>4</sub>, respectively. The accuracy of the  $K$  values were estimated to be  $\pm 8$  ppm, where the uncertainty results from an incomplete reduction of the strong dipolar interaction in the MAS experiment, mainly between the boron nuclei. These values of  $K$  are much smaller than those observed in MgB<sub>2</sub>, where  $K(^{11}\text{B}) = 100$  ppm [36] and in YNi<sub>2</sub>B<sub>2</sub>C, where  $K(^{11}\text{B}) \approx 400$  ppm [37] (both values are for room temperature). This comparison indicates that the values for the densities of states (DOS) at the Fermi level for the boron sites are much lower than those in the borides mentioned above. Especially the lack of *s*-type DOS, which is usually the contribution with the largest hyperfine field, reduces significantly the shifts. Indeed, the *s*-type DOS per boron atom is, in YB<sub>6</sub> [38], over 20 times smaller than in MgB<sub>2</sub> [38]. Also the *p*-type DOS per B atom is significantly smaller in YB<sub>6</sub> compared to MgB<sub>2</sub>. These data are compatible with the present electronic band structure calculations (see next Section) which show that *s*- and *p*-type boron states are located mainly below the Fermi energy and thus the contribution to the DOS at the  $E_F$  is small.

## 4 Electronic structure and chemical bonding

The first theoretical investigation of metal borides of general formula  $MB_6$  has been performed fifty years ago by Longuet-Higgins and Roberts [39] using the tight-binding approximation. According to these authors the octahedral arrangement of the B atoms leads to ten bonding states which, when filled with the 18 B  $s$  and  $p$  plus two metal valence electrons, will correspond to an insulator. A metal will be obtained when the hexaboride of a trivalent metal is considered instead of a divalent metal. In their paper the states below the Fermi level are not only characterized in terms of their bonding or antibonding properties but also as regards their participation in bonds within a single  $B_6$  octahedron or between neighbouring octahedra. Later [40] the higher lying valence and conduction bands of  $YB_6$  have been calculated by a discrete variational method in a non-selfconsistent fashion. Recent electronic-structure calculations for  $YB_6$  can be found in Ref. [2] (DOS only) and in Ref. [38] where also the band structure is given. For  $YB_4$  only the DOS has been published so far [2,38]. In both references, however, the lowest B  $2s$  band is not shown although it is of crucial importance for the chemical bonding in both borides as will be argued below. In the case of  $YB_6$  Shein et al. [38] designate it erroneously as “quasi-core B  $2s$  band” – obviously mainly because it is a low-lying band. In Fig. 2 the band structures for  $YB_4$  and  $YB_6$  are presented.

The DOS curves for  $YB_4$  and  $YB_6$  are given in Fig. 3 together with the local partial DOS components. For both borides the states at energies of ca.  $-15$  eV are dominated by B  $2s$  character with a considerable amount of B  $2p$  character. Such states appear for all B atoms constituting the  $B_6$  octahedra, but not for B(2), which belongs to the  $B_2$  unit of which each B atom is linked to two different octahedra. In this energy range hybrid orbitals are formed which lead to strong covalent  $\sigma$  bonds between the boron atoms within a  $B_6$  unit which can be seen from the corresponding electron densities shown in Fig. 4.

After an energy gap of about 3.7 eV a complex of bands appears in both compounds where in the lower energy range B  $s$  states prevail with an admixture of B  $p$  states except for the B(2) atoms. These states correspond mainly to bonds between different B<sub>6</sub> octahedra and  $s$ - $s$   $\sigma$  bonds in the B<sub>2</sub> units of YB<sub>4</sub>. At higher energies below the Fermi level B  $p$  states are predominant apart from a relatively small B  $s$  and a considerable Y  $d$  contribution. Also in this energy range the interoctahedral bonds are dominant except for the region very near the Fermi level in YB<sub>6</sub> where the intraoctahedral B-B bonds again become important.

In YB<sub>6</sub> the Y  $d$  states have mostly  $e_g$  character which can be seen from the valence electron densities in Fig. 5. This Figure also shows that this is not the case for YB<sub>4</sub> although near the Fermi level  $e_g$ -like character, i. e., ( $d_{z^2}, d_{x^2-y^2}$ ) character, is predominant.

Our results for YB<sub>6</sub> are in very good agreement with the detailed semiempirical tight-binding investigation by Longuet-Higgins and Roberts [39]. In order to make the comparison we performed crystal-field splittings for the B  $p$  (and Y  $d$ ) states. We thus obtained the distinction between their radial ( $p_z$ ) and tangential orbitals ( $p_x, p_y$ ). Together with electron-density plots for certain energy ranges, the regions for the different site orbitals for the B<sub>6</sub> octahedron could be identified. We obtained the following order (increasing energy):  $a_{1g}$  (band at ca. -15 eV),  $a'_{1g}$ ,  $t_{1u}$ ,  $e'_g$ , and  $t_{2g}$ . (The nomenclature is taken from Ref. [39] and refers to the irreducible representations for the whole octahedron.)

In Fig. 6 the valence electron densities in the (001) plane through the B atoms in YB<sub>4</sub> and YB<sub>6</sub> is displayed. Apart from the structural differences between both borides (irregular heptagonal arrangement of the B atoms outside the octahedra in YB<sub>4</sub> compared to an almost regular octagon in YB<sub>6</sub>) the slightly higher valence electron densities between the B atoms outside the octahedra

in both compounds can be seen as well as the deep density minima which designate the much weaker covalent Y–Y bonds perpendicular to the (001) plane.

## 5 Summary

For  $\text{YB}_4$  and  $\text{YB}_6$  we have performed electric-field gradient and Knight shift measurements for the B sites. The aim of the paper has been a comparison of the NMR results and the available structural data with the results of accurate first-principles calculations. We have therefore optimized the structures by atomic forces and stress-tensor minimization. For the optimized structures EFG calculations have been performed. Perfect agreement was found between the experimental and calculated structural parameters and electric-field gradients thus confirming the structure models available in the literature. Based on calculated total and local partial DOS as well as electron-density plots, we analyse the bonding situation in both compounds and conclude that the lowest valence bands are of particular importance for the stability of both yttrium borides.

## Acknowledgements

The authors would like to thank P. Vajda for stimulating discussions and the Austrian Science Foundation (project no. P15801-N02) for financial support. The calculations were performed on the Schrödinger II Linux cluster of the Vienna University Computer Centre.

## References

- [1] B. T. Matthias, T. H. Geballe, K. Andres, E. Corenzwit, G. W. Hull, J. P. Maita, *Science* 159 (1968) 530.
- [2] Y. Imai, M. Mukaida, M. Ueda, A. Watanabe, *Intermetallics* 9 (2001) 721.
- [3] O. J. Żogał, W. Wolf, P. Herzig, A. H. Vuorimäki, E. E. Ylinen, P. Vajda, *Phys. Rev. B* 64 (2001) 214110.
- [4] W. Wolf and P. Herzig, *Phys. Rev. B* 66 (2002) 224112.
- [5] W. Wolf and P. Herzig, *J. Alloys Comp.* 356–357 (2003) 73.
- [6] T. Ohno, Y. Kishimoto, T. Kanashiro, S. Kunii, *Czech. J. Phys.* 46 (1996) Suppl. S2, 787.
- [7] [http://cms.mpi.univie.ac.at/vasp/;](http://cms.mpi.univie.ac.at/vasp/)  
<http://materialsdesign.com/Pages/VASP.htm>
- [8] G. Kresse, J. Furthmüller, *Phys. Rev. B* 54 (1996) 11169.
- [9] G. Kresse, J. Furthmüller, *Comput. Mater. Sci.* 6 (1996) 15.
- [10] P. Hohenberg, W. Kohn, *Phys. Rev.* 136 (1964) B 864.
- [11] W. Kohn, L. J. Sham, *Phys. Rev.* 140 (1965) A 1133.
- [12] P. E. Blöchl, *Phys. Rev. B* 50 (1994) 17953.
- [13] G. Kresse, D. Joubert, *Phys. Rev. B* 59 (1998) 1758.
- [14] J. P. Perdew, J. A. Chevary, S. H. Vosko, K. A. Jackson, M. R. Pederson, D. J. Singh, C. Fiolhais, *Phys. Rev. B* 46 (1992) 6671.
- [15] A. Guette, M. Vlasse, J. Etourneau, R. Naslain, *C. R. Acad. Sc. Paris, Ser. C* 291 (1980) 145.
- [16] H. P. Klesnar, P. Rogl, *High Temp.-High Press.* 22 (1990) 453.
- [17] N. N. Zhuravlev, I. A. Belousova, R. M. Manelis, N. A. Belousova, *Sov. Phys. Crystallogr.* 15 (1971) 723 [*Kristallografiya* 15 (1970) 836].

- [18] F. Binder, *Radex-Rdsch.* 1977, 52.
- [19] M. Korsukova, Proc. 11th Int. Symp. Boron, Borides, and Related Compounds, Tsukuba, 1993, *JJAP Series* 10 (1994) 15.
- [20] Y. Takahashi, K. Ohshima, F. P. Okamura, S. Otani, T. Tanaka, *J. Phys. Soc. Jpn.* 68 (1999) 2304.
- [21] O. K. Andersen, *Phys. Rev. B* 12 (1975) 3060.
- [22] D. D. Koelling, G. O. Arbman, *J. Phys. F: Metal Phys.* 5 (1975) 2041.
- [23] E. Wimmer, H. Krakauer, M. Weinert, A. J. Freeman, *Phys. Rev. B* 24 (1981) 864.
- [24] H. J. F. Jansen, A. J. Freeman, *Phys. Rev. B* 30 (1984) 561.
- [25] B. I. Min, T. Oguchi, H. J. F. Jansen, A. J. Freeman, *J. Magn. Magn. Mat.* 54–57 (1986) 1091.
- [26] L. Hedin, B. I. Lundqvist, *J. Phys. C: Solid St. Phys.* 4 (1971) 2064.
- [27] L. Hedin, S. Lundqvist, *J. Phys. (Paris)* 33 (1972) C3-73.
- [28] P. Herzig, *Theoret. Chim. Acta.* 67 (1985) 323.
- [29] P. Blaha, K. Schwarz, P. Herzig, *Phys. Rev. Lett.* 54 (1985) 1192.
- [30] P. Blaha, K. Schwarz, P. H. Dederichs, *Phys. Rev. B* 37 (1988) 2792.
- [31] D. Massiot, F. Fayon, M. Capron, I. King, S. Le Calve, B. Alonso, J.-O. Durand, B. Bujoli, Z. Gan, G. Hoatson, *Magn. Reson. Chem.* 40 (2002) 70.
- [32] H. Nöth, B. Wrackmeyer, in *NMR Basic Principles and Progress*, vol. 14, edited by P. Diehl, E. Fluck, R. Kosfeld, (Springer, 1978), p. 1.
- [33] D. Sundholm, J. Olsen, *J. Chem. Phys.* 94 (1991) 5051.
- [34] P. Pyykkö, *Z. Naturforsch.* 47a (1992) 189.
- [35] K. Schwarz, H. Ripplinger, P. Blaha, *Z. Naturforsch.* 51a (1996) 527.
- [36] A. P. Gerashenko, K. N. Mikhalev, S. V. Verkhovskii, A. E. Karkin, B. N. Goshchitskii, *Phys. Rev. B* 65 (2002) 132506.



- [37] B. J. Suh, F. Borsa, D. R. Torgeson, B. K. Cho, P. C. Canfield, D. C. Johnston, J. Y. Rhee, B. N. Harmon, Phys. Rev. B 54 (1996) 15341.
- [38] I. R. Shein, S. V. Okatov, N. I. Medvedeva, A. L. Ivanovskii, cond-mat/0202015 (2002).
- [39] H. C. Longuet-Higgins, M. de V. Roberts, Proc. R. Soc. London 224 (1954) 336.
- [40] P. F. Walch, D. E. Ellis, F. M. Mueller, Phys. Rev. B 15 (1977) 1859.

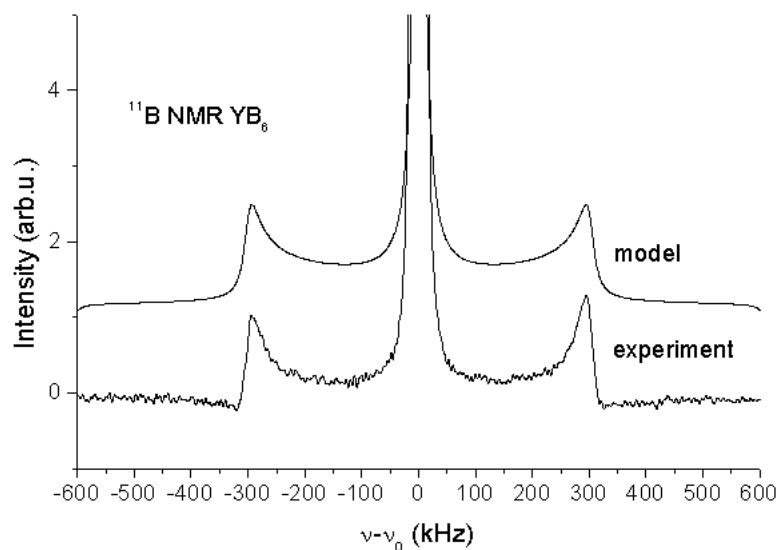
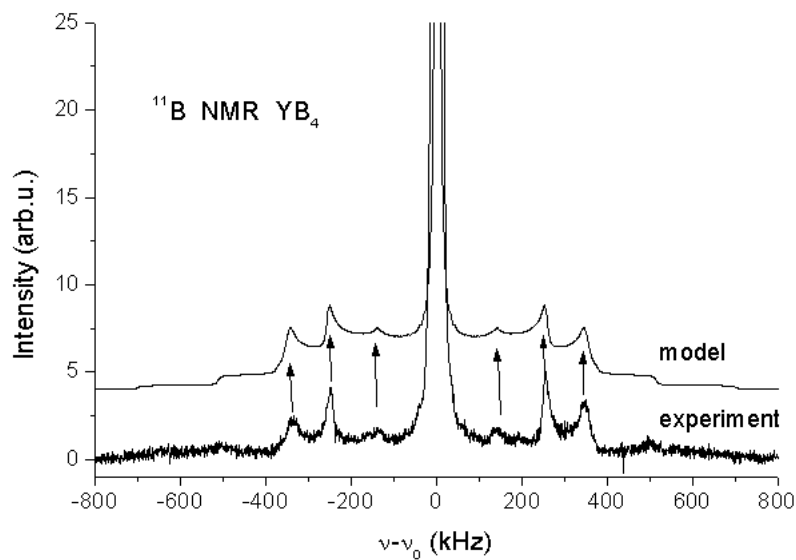


Fig. 1. Experimental and theoretical (model) powder-pattern <sup>11</sup>B spectrum for YB<sub>4</sub> (top) and YB<sub>6</sub> (bottom). For better readability the model spectra are shifted up with respect to the experimental ones. For YB<sub>4</sub> the arrows indicate positions of 90° singularities ( $\eta \sim 0$ ) for B(2) (outermost arrows) and B(1) (middle arrows) except for the singularity for B(3) (innermost arrows) where the angle is different from 90° ( $\eta = 0.46$ ).

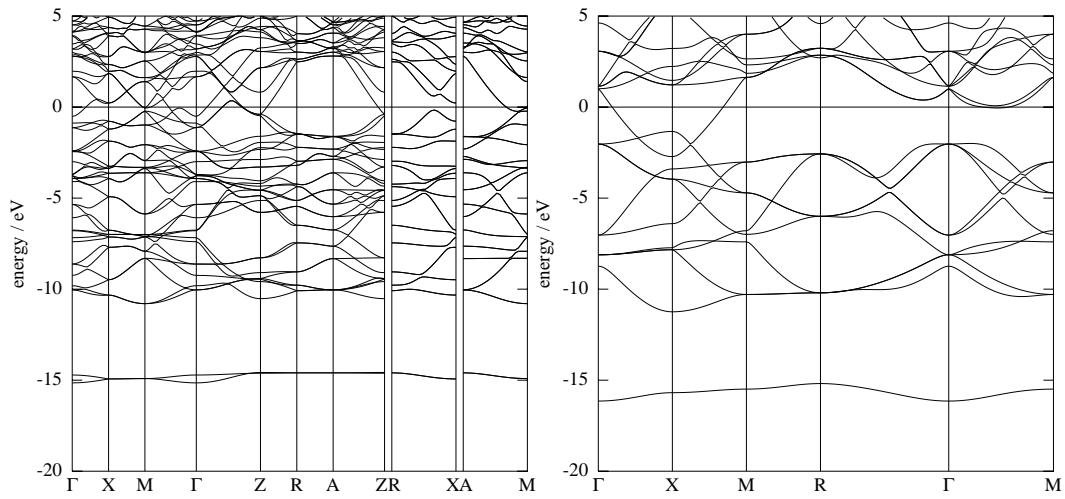


Fig. 2. Electronic band structure for  $\text{YB}_4$  (left) and  $\text{YB}_6$  (right).

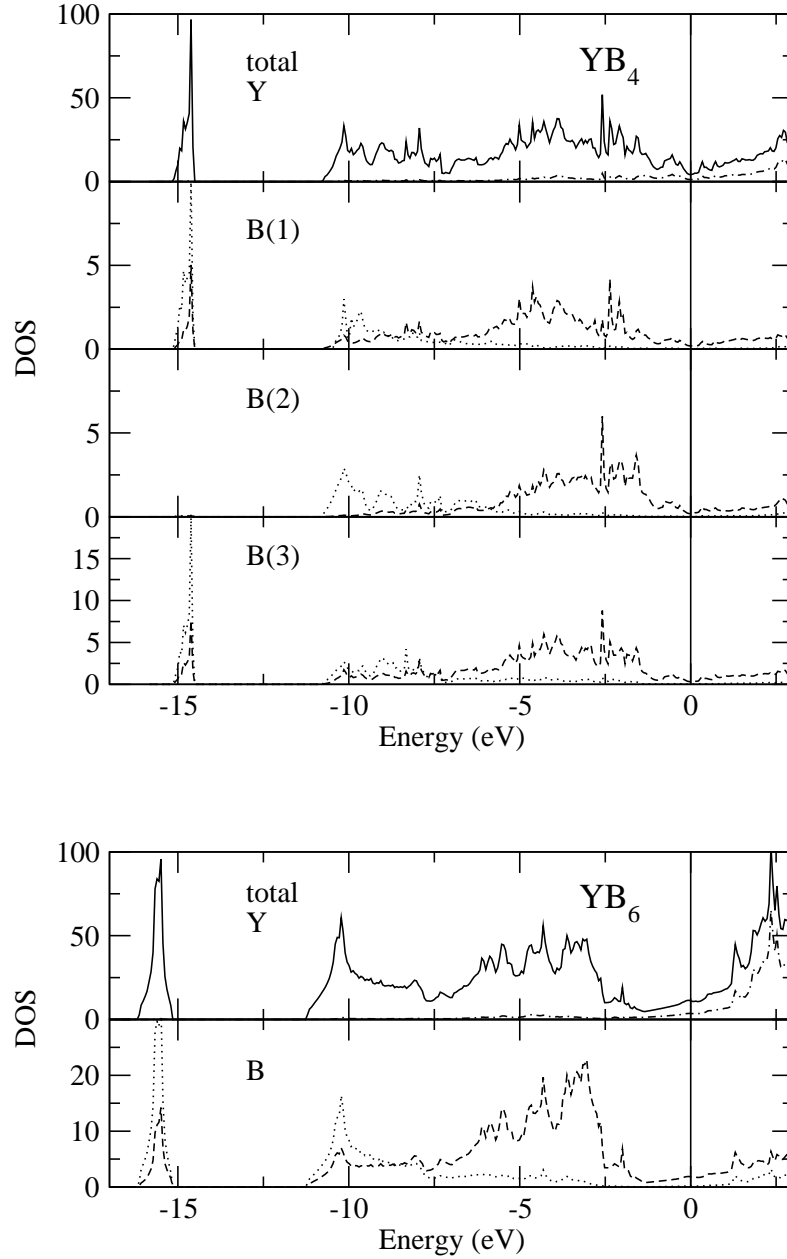


Fig. 3. Total DOS (full line) and local partial DOS components (B  $s$ : dotted line; B  $p$ : dashed line; Y  $d$ : dash-dotted line) for  $\text{YB}_4$  (top) and  $\text{YB}_6$  (bottom) in units of states per Rydberg and per formula unit.

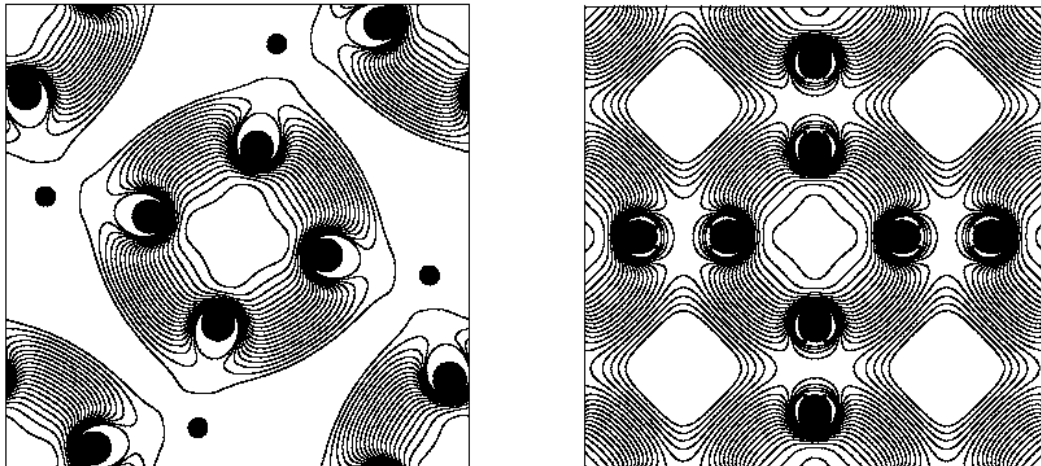


Fig. 4. Electron densities in the (001) plane through the B atoms for the lowest valence bands at ca.  $-15$  eV. Left:  $\text{YB}_4$ , right:  $\text{YB}_6$ . A logarithmic grid of contour lines has been used ( $x_i = x_0 2^{i/3}$ ). For  $\text{YB}_4$  the B(2) atoms appear as black bullets without a surrounding electron density.

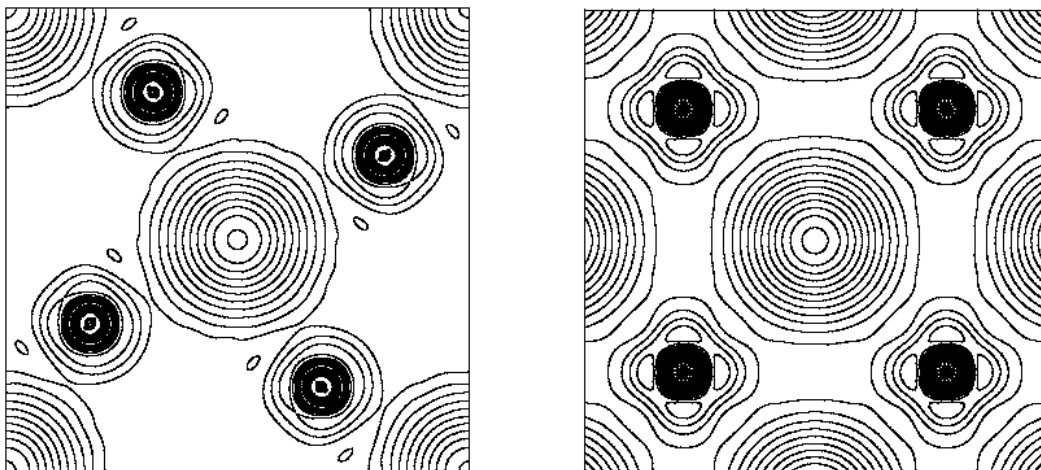


Fig. 5. Valence electron densities in the (001) plane through the Y atoms. Left:  $\text{YB}_4$ , right:  $\text{YB}_6$ . A logarithmic grid of contour lines has been used ( $x_i = x_0 2^{i/3}$ ).

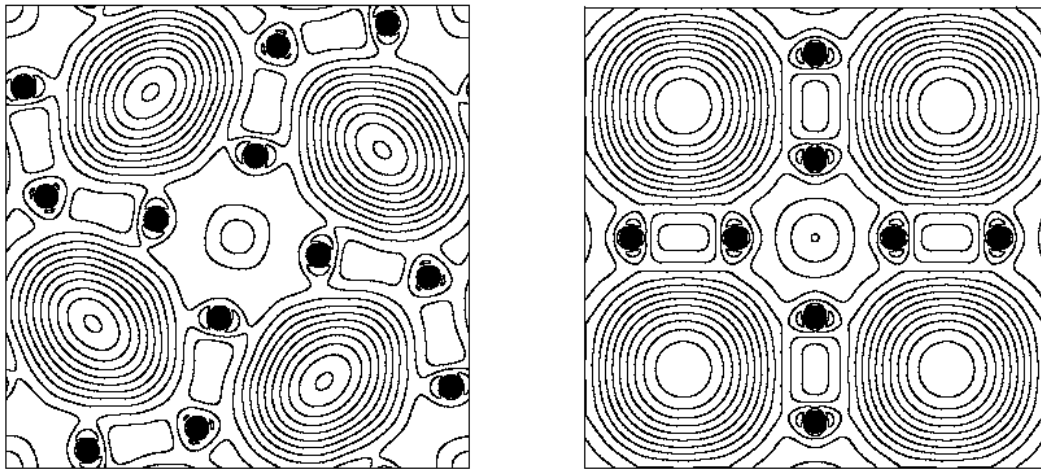


Fig. 6. Valence electron densities in the (001) plane through the B atoms. Left:  $\text{YB}_4$ , right:  $\text{YB}_6$ . A logarithmic grid of contour lines has been used ( $x_i = x_0 2^{i/3}$ ).